1999

# Fundamental problems in coastal ocean prediction

Chu, Peter C.

Chu, P.C., 1999: Fundamental problems in coastal ocean prediction. Proceedings of Oceanology International 99 (Keynote Paper), 37-46
https://hdl.handle.net/10945/36285

# FUNDAMENTAL PROBLEMS IN COASTAL OCEAN PREDICTION

Dr. Peter C. Chu
Department of Oceanography, Naval Postgraduate School, Monterey, CA 93943, USA

## 1 INTRODUCTION

Several major problems, namely, uncertain surface forcing, unknown open boundary conditions (OBC), and pressure gradient error using the $\sigma$-coordinate, restrict the accuracy of littoral zone ocean prediction.

The littoral zone ocean prediction is usually proceeded by integrating a set of dynamic/thermodynamic equations from initial states under the surface wind forcing

$$\rho_0 K_M(\partial u/\partial z, \partial v/\partial z)_{z=0} = (\tau_{0x}, \tau_{0y}) \qquad (1)$$

the surface thermal forcing

$$K_H \frac{\partial T}{\partial z}|_{z=0} = \alpha_1(\frac{Q_H}{\rho c_p}) + \alpha_2 \kappa (T_{OBS} - T_0), \qquad (2)$$

$$K_S \frac{\partial S}{\partial z}|_{z=0} = \alpha_1 Q_S + \alpha_2 \kappa (S_{OBS} - S_0) \qquad (3)$$

and the lateral boundary conditions. Here $(u, v)$ and $(\tau_{0x}, \tau_{0y})$ are the two components of the water velocity and wind stress vectors, $T_{OBS}$ and $S_{OBS}$ are the observed temperature and salinity, $T_0$ and $S_0$ are the surface temperature and salinity, $c_p$ is the specific heat, and $Q_H$ and $Q_S$ are surface net heat and salinity fluxes, respectively. The coupling coefficient $\kappa$ is the reciprocal of the restoring time period for a unit volume of water. The parameters $(\alpha_1, \alpha_2)$ are (0,1)-type switches: $\alpha_1 = 1$, $\alpha_2 = 0$, would specify the flux forcing; $\alpha_1 = 0$, $\alpha_2 = 1$, would specify the restoring-type forcing. The restoring-type forcing, called Haney-type surface boundary condition (Haney, 1971), was obtained under the assumption that the ocean is in contact with an atmospheric equilibrium state (i.e., an atmosphere with a near-infinite heat capacity). The validity of the restoring-type condition need to be verified.

At open lateral boundaries where the numerical grid ends, the fluid motion should be unrestricted. Ideal open boundaries are transparent to motions. Two approaches, local-type and inverse-type are available for determining OBC. The local-type approach is to select an OBC from a set of *ad hoc* OBCs, which will introduce inaccuracies into a numerical solution (Chapman 1985). The inverse-type approach is to determine the OBC from a "best" fit between model solutions and interior observations. The most popular and successful scheme for this approach is an adjoint method (Robinson, 1993; Seiler 1993; Gunson and Malanotte-Rizzoli 1996). The disadvantages that may restrict use of adjoint method are: ocean-model dependency of the adjoint equation, and difficulty in deriving the adjoint equation when the model contains rapidly changing (discontinuous) processes, such as ocean mixed layer dynamics. To overcome such deficiencies, Chu et al. (1997) have developed an inverse method to determine OBCs of **any ocean model** from interior observations by seeking a relationship among three vectors: open boundary parameter vector (**B**), observation vector (**O**), and solution vector (**S**).

How to reduce the horizontal pressure gradient error is another key issue of using $\sigma$-coordinate ocean models, especially of using coastal models. The error is caused by the splitting of the horizontal pressure gradient term into two parts and the subsequent incomplete cancellation of the truncation errors of those parts. Due to the fact that the higher the order of the difference scheme, the less the truncation error and the more complicated the computation, Chu and Fan (1997a,b; 1998) have used and developed several high-order schemes for ocean models without drastic increase of CPU time.

## 2 MODEL PREDICTABILITY

Ocean numerical models are usually initial-value and/or boundary-value problems. Change in either initial or boundary condition leads to a variation of model solutions. Much of the predictability research has been done on the response of model behavior to an initial value perturbation. Little effort has been made to study the response of model behavior to a boundary value perturbation.

## 2.1 Lorenz System

Recently, Chu (1999) used the Lorenz system (Lorenz, 1963)

$$\frac{dX}{d\tau} = -\sigma X + \sigma Y, \tag{4}$$

$$\frac{dY}{d\tau} = -XZ + rX - Y \tag{5}$$

$$\frac{dZ}{d\tau} = XY - bZ. \tag{6}$$

to discuss two kinds of predictability, the model sensitivity to inaccurate initial conditions (first kind) and to inaccurate boundary conditions (second kind). Chu (1999) found that the boundary condition error is transferred into the parameter error in $r$.

Chu (1999) integrated the Lorenz system (4)-(6) under three different cases: the control run, the sensitivity to initial condition run, and the sensitivity to boundary condition run. The value $\Delta\tau$ is chosen as 0.01 for the dimensionless time increment. All the three cases are integrated from $\tau = 0$ to $\tau = 50$.

## 2.2 Sensitivity Study

### 2.2.1 Control Run

The control run is to use the same initial conditions

$$X^{(C)}(0) = 0,\ Y^{(C)}(0) = 1,\ Z^{(C)}(0) = 0 \tag{7}$$

and the same values for model parameters,

$$r^{(C)} = 28,\ \sigma^{(C)} = 10,\ b^{(C)} = \frac{8}{3} \tag{8}$$

as Lorenz (1963).

### 2.2.2 Sensitivity to Initial Error Run

The sensitivity to initial error run (indicated by the superscript '$I$') is to keep everything the same as the control run except the initial conditions,

$$X^{(I)}(0) = 0,\ Y^{(I)}(0) = Y^{(C)}(0)(1+\varepsilon),\ Z^{(I)}(0) = 0 \tag{9}$$

where we introduce a small error $\varepsilon$ ($= 10^{-4}$) in the initial condition.

### 2.2.3 Sensitivity to Boundary Error Run

The sensitivity to boundary error run (indicated by the superscript '$B$') is to keep everything the same as the control run except the parameter $r$,

$$r^{(B)} = r^{(C)}(1+\varepsilon) \tag{10}$$

where we introduce a small error $\varepsilon$ ($= 10^{-4}$) in the parameter $r$.

## 2.3 Model Error Growth

The model error growth due to initial condition error, boundary condition error, or both can be obtained from the time evolution of the difference between the sensitivity runs and the control run. Thus, we use

$$E^{(S)}(\tau) = \frac{\sqrt{[\Delta X(\tau)]^2 + [\Delta Y(\tau)]^2 + [\Delta Z(\tau)]^2}}{\sqrt{\left[X^{(C)}(\tau)\right]^2 + \left[Y^{(C)}(\tau)\right]^2 + \left[Z^{(C)}(\tau)\right]^2}} \tag{11}$$

to detect the model error growth. Here $S = I, B$, and

$$\Delta X(\tau) = X^{(S)}(\tau) - X^{(C)}(\tau)$$

$$\Delta Y(\tau) = Y^{(S)}(\tau) - Y^{(C)}(\tau)$$

$$\Delta Z(\tau) = Z^{(S)}(\tau) - Z^{(C)}(\tau)$$

The model error evolution shows a similar pattern for the two cases: a growing period and an oscillation period (Figure 1). During the growing period, the model error $E^{(S)}(\tau)$ increases from 0 at $\tau = 0$ to an evident value $\left[E^{(S)}(\tau) > 1\right]$ at certain value of $\tau$, which is called the error growing period. During the oscillation period, $E^{(I)}(\tau)$ oscillates between 4.5 and 0.1, and $E^{(B)}(\tau)$ oscillates between 5.0 and 0.2. We may also notice that the error growing period and magnitudes are comparable between $E^{(I)}(\tau)$ and $E^{(B)}(\tau)$. The dimensionless growing period is around 22 for both errors. Thus, preparation of accurate boundary conditions has the same importance as preparation of accurate initial conditions.

# 3 Surface Forcing Uncertainty

To verify the validity of Haney-type surface thermal boundary conditions, Chu and his colleagues computed cross correlation coefficient (CCC) between $Q_H$ and $\Delta T$ [$= (T_{OBS} - T_0)$] using the NCEP global re-analyzed data (six hour resolution) during 1 October 1994 - 31 December 1995 and using a coupled atmosphere-ocean model developed at the Institute for Space Studies at NASA/Goddard Space Flight Center (Chu, et al., 1998a). The ensemble mean CCC fields show (a) no correlation between $Q$ and $\Delta T$ in the equatorial and coastal regions, and (b) evident correlation (CCC $\geq$ 0.7) between $Q$ and $\Delta T$ in the middle and high latitude open ocean regions. The variance analysis suggests a value of 70 $\mathrm{Wm^{-2}K^{-1}}$ (65 $\mathrm{Wm^{-2}K^{-1}}$) for the coefficient $\kappa$ in the northern (southern) middle and high latitude zone.

To investigate the uncertainty in the surface wind forcing and its effect on the coastal prediction, the Princeton Ocean Model (POM) developed by Blumberg and Mellor (1987) was used with 20 km horizontal resolution and 23 sigma levels conforming to a realistic bottom topography during the life time of tropical cyclone Ernie 1996

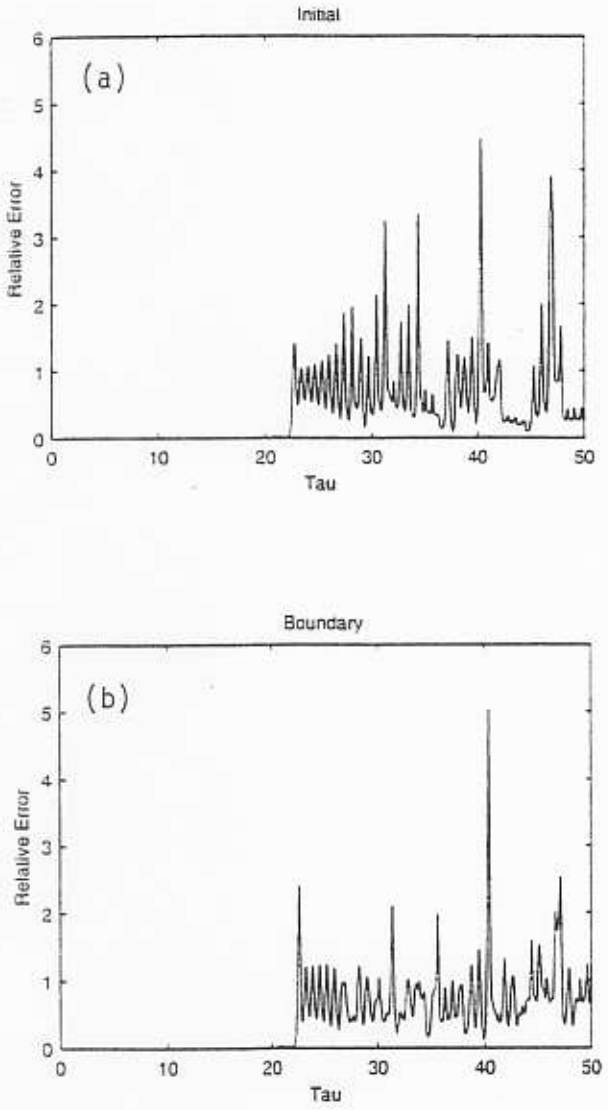


**Figure 1 – Time evolution of (a) initial condition error, and (b) boundary condition error.**

(Figure 2) over the South China Sea (SCS). Numerical integration was divided into pre-experimental and experimental stages. During the pre-experimental stage, the POM was integrated for 43 months from zero velocity and April temperature and salinity climatological fields with climatological monthly mean wind stresses, restoring type surface salt and heat, and observational oceanic inflow/outflow at the open boundaries. The fields at the end of the integration period were taken as the initial fields (1 November) for the sensitivity study. During the experimental stage, the POM was integrated for another month under the NCEP re-analyzed surface fluxes along with two surface wind data sets: namely, the daily averaged interpolated NASA Scatterometer (NSCAT) winds and the NCEP winds. All the surface forcing data used were from 1 to 30 November 1996. The study (Chu, et al, 1998c) shows that the root-mean-square (RMS) difference of each component (zonal or latitudinal) between the two wind data over the whole SCS during November 1996 fluctuated between 2.7 m/s to 6.5 m/s (Figure 3). The uncertainty of the whole SCS response to the two wind data sets were 4.4 cm for surface elevation (Figure 4a), 0.16 m/s for surface current velocity (Figure 4b), and 0.5°C for near-surface temperature (Figure 4c), respectively.

## 4 Jacobian Matrix Method for Determining OBCs

Improvement of the prediction partially depends on the determination of lateral OBCs. If $r$ denotes the position of any point along the open boundary $\Gamma$, the boundary values of any variable $\eta$ is a function of $r$, $\eta^{(b)} = \eta^{(b)}(r)$. Let $f_1(r), f_2(r), ..., f_n(r)$ be a series of known basis functions. We expand the function $\eta^{(b)}(r)$ into

$$\eta^{(b)}(r) = \sum_{i=1}^{n} b_i f_i(r) \tag{12}$$

Thus, the determination of the open boundary condition $\eta^{(b)}(r)$ becomes the determination of an n-dimensional boundary vector $\mathbf{B} = (b_1, b_2, ..., b_n)$. Assume that there are $m$ observations, forming an m-dimensional vector (observation vector) $\mathbf{O} = (O_1, O_2, ...O_m)$, located at the interior (Figure 5). If $\mathbf{B}$ is given, we can solve the dynamic system and obtain the solution $S$. At the same locations where the observations take place, the solutions form a solution vector $\mathbf{S} = (S_1, S_2, ...S_m)$. Notice that the dimension of $\mathbf{B}$ is not necessary the same as the dimension of $\mathbf{O}$ and $\mathbf{S}$.

The optimization method is used to find $\mathbf{B} = (b_1, b_2, ..., b_n)$ by minimize the root-mean-square (RMS) error

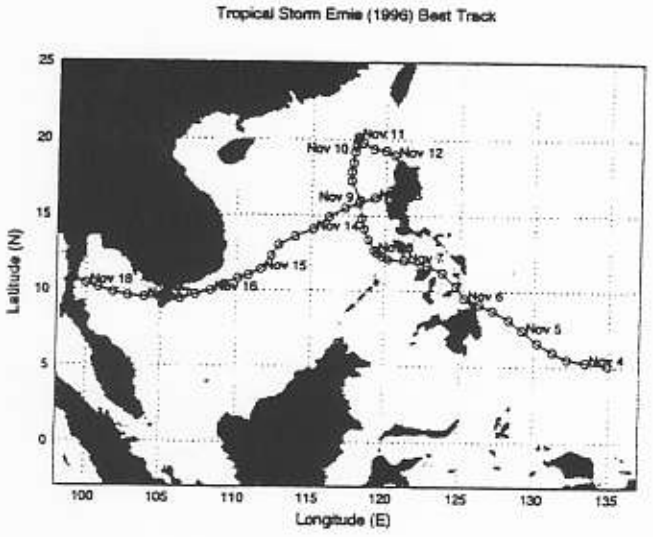


Figure 2 – The track of the tropical cyclone Erni 4-18 November, 1996 (from Chu et al., 1998b)

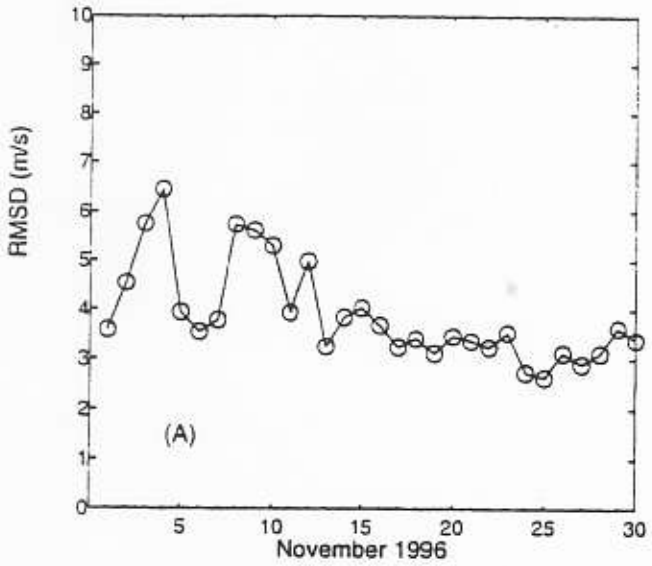


Figure 3 – Temporally varying root-mean-square difference between daily mean NSCAT and NCEP winds over the South China Sea (from Chu et al., 1998b)

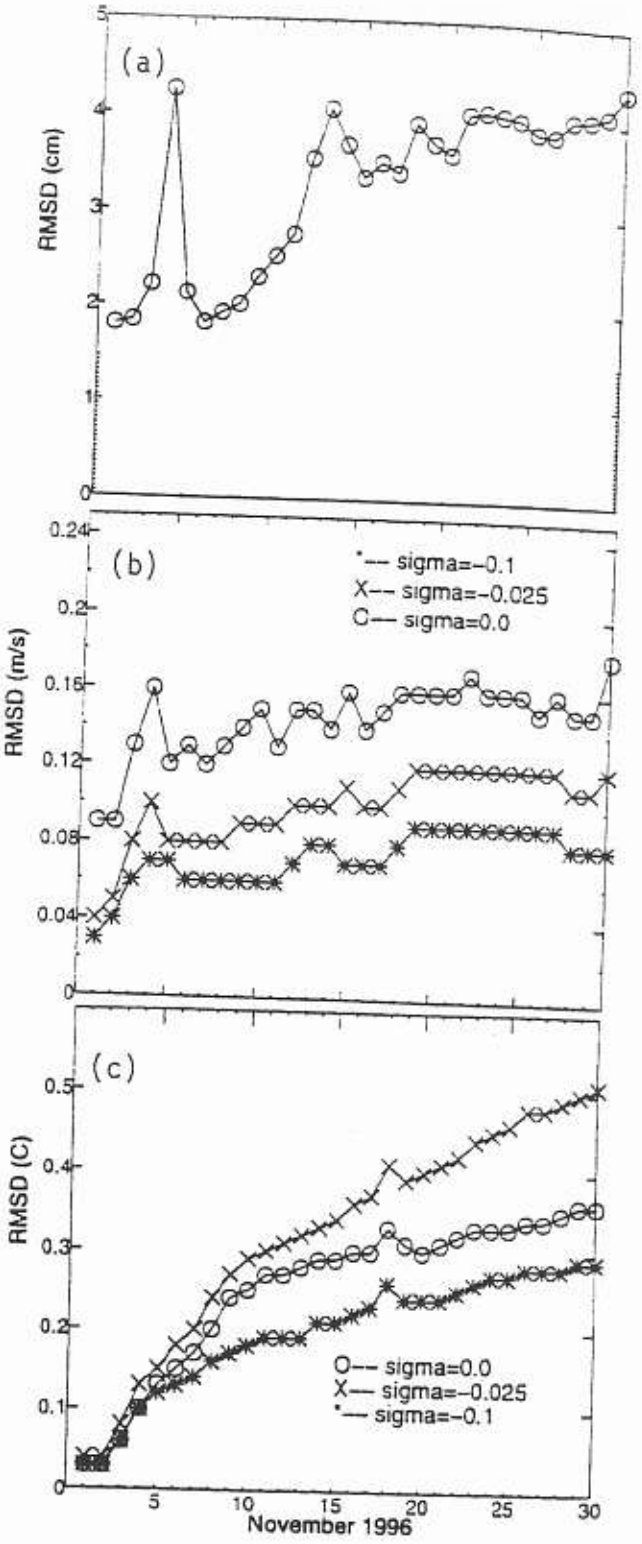


Figure 4 – Temporally varying root-mean-square difference between model results under two kinds of wind forcing over the whole South China Sea (from Chu et al., 1998b): (a) surface elevation, (b) velocity, and (c) temperature.

$$I = \sqrt{\frac{1}{m}\sum_{j=1}^{m}(S_j - O_j)^2}. \qquad (13)$$

This method was verified by a flat bay centered at 35°N and bounded by three rigid boundaries (Chu et al., 1997). This bay expands 1000 km in both the north-south and east-west directions. The northern, southern, and western boundaries are rigid, and the eastern boundary is open. Using the optimization method, the temporally varying OBC, $\mathbf{B}(t)$, is determined. After 10 day's of integration, the magnitude of relative error $E^{(O)}$ is on the order of $10^{-4}$-$10^{-5}$ (Figure 6). Chu et al. (1997) also pointed out that smoothing on $\delta\mathbf{B}$ is very important for this method. This optimization method performs well even when random noises are added to the 'observational' points. This indicates that we can use real-time data to invert for the unknown open boundary values.

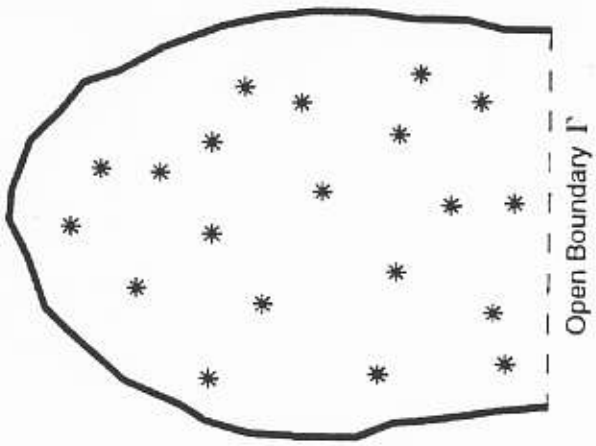


**Figure 5 – Can open boundary condition be determined from interior values? (from Chu et al., 1997)**

# 5 Basin/Coastal Nested Modeling

One of the difficult problems in marginal sea modeling is the uncertainty of the open boundary condition (OBC). Three approaches, local-type, inverse-type, and nested basin/coastal modeling are available for determining OBC. The third approach is to use nested basin/coastal model: integration of the basin model provides the OBC for the coastal model. In this study, we will use the nested Princeton Ocean Model (POM) developed by *Blumberg and Mellor* [1987] to simulate the east Asian regional sea circulation and thermohaline structure.

## 5.1 Model Description

Here, we use a rectilinear grid with horizontal spacing of 1° by 1° for the North Pacific basin model, and of 0.25° by 0.25° for the regional model (Figure 7). Both models have 23 vertical sigma coordinate levels and use realistic bathymetry data from the Naval Oceanographic Office DBDB5 database (5 minute by 5 minute resolution). The basin model domain is 80°E - 90°W, 30°S - 65°N, and the regional model domain is 98° - 143°E, 0° - 50°N. The barotropic (baroclinic) mode time steps are 50 s and 25 s (1800 s and 900 s) for basin and coastal models, respectively. The horizontal diffusivities are modeled using the *Smagorinsky* [1963] form with the coefficient chosen to be 0.2 for this application. The bottom stress is assumed to follow a quadratic law and the drag coefficient is specified as 0.0025 [*Blumberg and Mellor*, 1987].

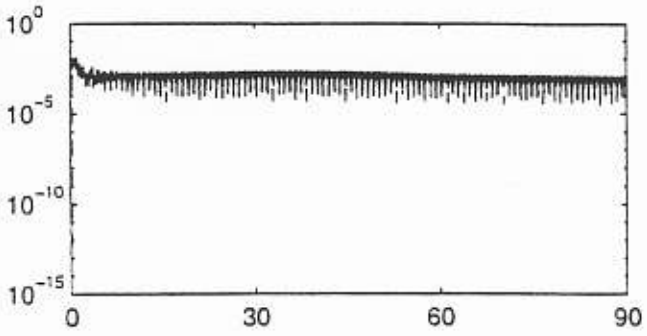


**Figure 6 – Relative error of the Jacobian Matrix method (from Chu et al., 1997).**

The surface wind and thermohaline forcing at each time step are interpolated from monthly mean climatological $Q_H$ and $Q_S$ $(= E - P)$ from the COADS, which was taken as the value at the middle of the month.

### 5.2 Lateral Boundary Conditions

Solid lateral boundaries, i.e., the modeled ocean bordered by land, were defined using a free slip condition for velocity and a zero gradient condition for temperature and salinity. No advective or diffusive heat, salt or velocity fluxes occur through these boundaries. Since we are interested in the regional model results, the OBCs for the basin model are set as rigid boundaries. OBCs for the coastal model are determined from the basin model output at each time step.

### 5.3 Model Initialization

The model year consists of 360 days (30 days per month), day 361 corresponds to 1 January. We integrated the nested POM model for seven years from zero velocity and January temperature and salinity climatological fields [*Levitus and Boyer*, 1994; *Levitus et al.*, 1994] with COADS monthly mean surface wind stress and salt and heat fluxes. We use the last four years' output for analysis.

### 5.4 Simulated Japan/East Sea (JES) Circulation

Velocity, temperature, and salinity at major straits (e.g., Tsushima, Taiwan, Luzon, and Karimata, etc.) are obtained from the nested POM model. The volume transports (Sv, 1 Sv = $10^6$ $m^3/s$) were computed for all the straits. The model simulates a reasonable upper level (30 m) JES circulation pattern (Figure 8).

## 6 High-Order Difference Schemes

### 6.1 A Hidden Problem

Improvement of the prediction also partially depends on the selection of the discretization schemes. Most coastal models use second-order difference schemes (such as second-order staggered C-grid scheme) to approximate first-order derivative (Blumberg and Mellor, 1987; Hadivogel et al., 1991)

$$\left(\frac{\partial p}{\partial x}\right)_i \simeq \frac{p_{i+1/2} - p_{i-1/2}}{\Delta} - \frac{1}{24}\left(\frac{\partial^3 p}{\partial x^3}\right)_i \Delta^2, \quad (14)$$

where $p$, $\Delta$ represent pressure and grid spacing. Such a difference scheme was proposed by numerical modelers in early 50's as the first generation computers came into place. Since then the computer updates rapidly with several orders of magnitude increase in computational power. However, the difference schemes used by most modelers now are still staying at the 50's level (second-order schemes). Besides, the current scheme uses the local Lagrangian Polynomials whose derivatives are discontinuous. Figure 9 shows the process of computing first-order derivative of function $\phi(x)$ at the grid $x_i$, $L'(x_i)$ is the tangential of the Lagrangian Polynomial. As $i$ increases, three neighboring Lagrangian Polynomials $L_{i-1}, L_i, L_{i+1}$ have different tangential at the point $x_i$. Such a hidden problem might distort the physical process. In a series papers, Chu and Fan (1997, 1998, 1999) have shown the advantage of using high-order schemes.

### 6.2 Combined Compact Scheme

Recently, Chu and Fan (1998, 1999) proposed a new three-point combined compact difference (CCD) scheme,

$$\left(\frac{\delta f}{\delta x}\right)_i + \alpha_1\left(\left(\frac{\delta f}{\delta x}\right)_{i+1} + \left(\frac{\delta f}{\delta x}\right)_{i-1}\right) + \beta_1 h\left(\left(\frac{\delta^2 f}{\delta x^2}\right)_{i+1} - \left(\frac{\delta^2 f}{\delta x^2}\right)_{i-1}\right) + \ldots = \frac{a_1}{2h}\left(f_{i+1} - f_{i-1}\right) \quad (15)$$

$$\left(\frac{\delta^2 f}{\delta x^2}\right)_i + \alpha_2\left(\left(\frac{\delta^2 f}{\delta x^2}\right)_{i+1} + \left(\frac{\delta^2 f}{\delta x^2}\right)_{i-1}\right) + \beta_2\frac{1}{2h}\left(\left(\frac{\delta f}{\delta x}\right)_{i+1} - \left(\frac{\delta f}{\delta x}\right)_{i-1}\right) + \ldots = \frac{a_2}{h^2}\left(f_{i+1} - 2f_i + f_{i-1}\right) \quad (16)$$

to compute $f_i'$ , $f_i'', \ldots f_i^{(k)}$ by means of the values and derivatives at the two neighboring points. Moving from the one boundary to the other, CCD forms a global algorithm to compute various derivatives at all grid points, and guarantees continuity of all derivatives at each grid point.

### 6.3 Seamount Test Case

#### 6.3.1 Model Description

Suppose a seamount located inside a periodic $f$-plane ( $f_0 = 10^{-4}s^{-1}$) channel with two solid, free-slip boundaries along constant $y$. Unforced flow over seamount in the presence of resting, level isopycnals is an idea test

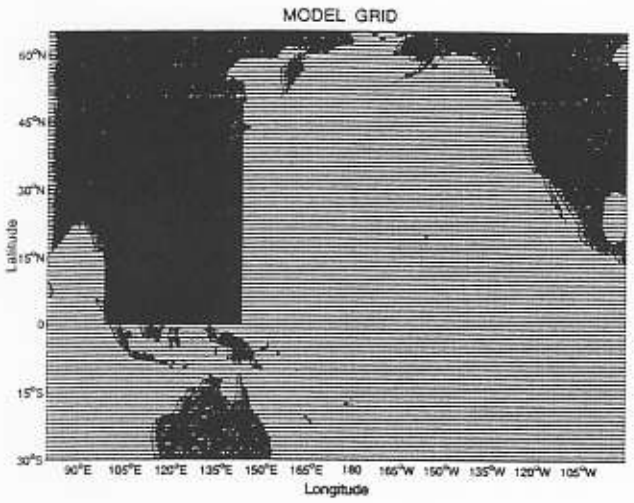


**Figure 7 – Nested grid points for the East Asian Marginal Sea (EAMS) studies.**

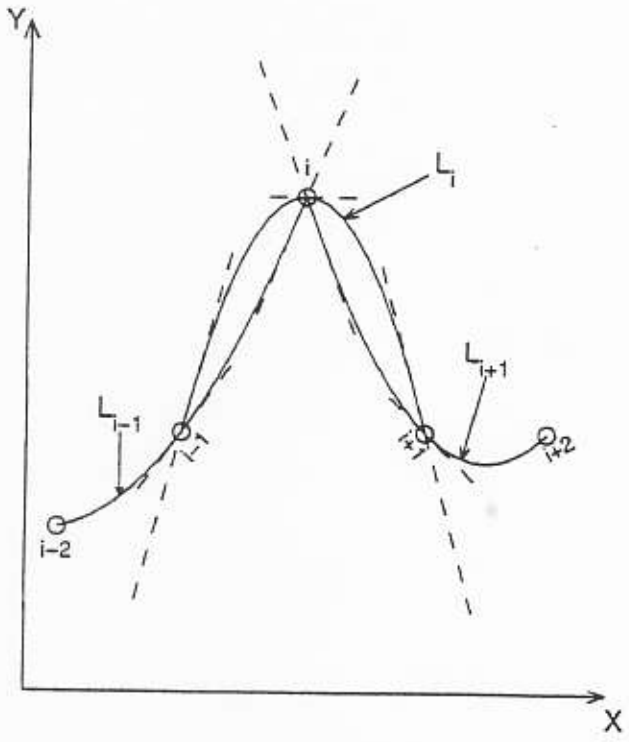


**Figure 9 – Discontinuity of the first derivatives of the Lagrangian Polynomials at each grid point.**

case for the assessment of pressure gradient errors in simulating stratified flow over topography. The flow is assumed to be reentrant (periodic) in the along channel coordinate (i.e., $x$-axis). We use this seamount case of the Semi-spectral Primitive Equation Model (SPEM) version 3.9 to test the new difference scheme. The reader is referred to the original reference (Haidvogel et al., 1991) and the SPEM 3.9 User's Manuel (Hedstrom, 1995) for detail information. The time step and grid size used here are,

$$\Delta t = 675 \text{ s}, \qquad \Delta x = \Delta y = 5 \text{ km}.$$

### 6.3.2 Topography

The domain is a periodic channel, 320 km long and 320 km wide. The channel walls are solid (no normal flow) with free-slip viscous boundary conditions. The channel has a far-field depth $h_{\max}$ and in the center includes an isolated Gaussian-shape seamount with a width $L$ and an amplitude $h_s$(Figure 10),

$$h(x,y) = h_{\max} - h_s \exp\left[-\frac{(x-x_0)^2+(y-y_0)^2}{L^2}\right] \quad (17)$$

where $(x_0, y_0)$ are the longitude and latitude of the seamount center. The far-field depth ($h_{\max}$) is fixed as 5,000 m. But the seamount amplitude ($h_s$) changes from 500 to 4,500 m, and the lateral scale of the seamount ($L$) varies from 10 to 40 km. for the study.

### 6.3.3 Density Field

The fluid is exponentially stratified and initially at rest. The initial density field has the form,

$$\rho_i = \overline{\rho}(z) + \widehat{\rho}\exp(\frac{z}{H\rho}) \quad (18)$$

where $z$ is the vertical coordinate, $H_\rho = 1000$ m, and

$$\overline{\rho}(z) = 28 - 2.\exp(\frac{z}{H\rho}) \quad (19)$$

is a reference density field.

## 6.4 Temporal Variations of Peak Error Velocity

Owing to a very large number of calculations performed, we discuss the results exclusively in terms of the maximum absolute value the spurious velocity (called peak error velocity) generated by the pressure gradient errors. Figure 11 shows the time evolution of the peak error velocity for the first 20 days of integration with the second-, fourth-, and sixth-order ordinary schemes. The peak error velocity fluctuates rapidly during the first

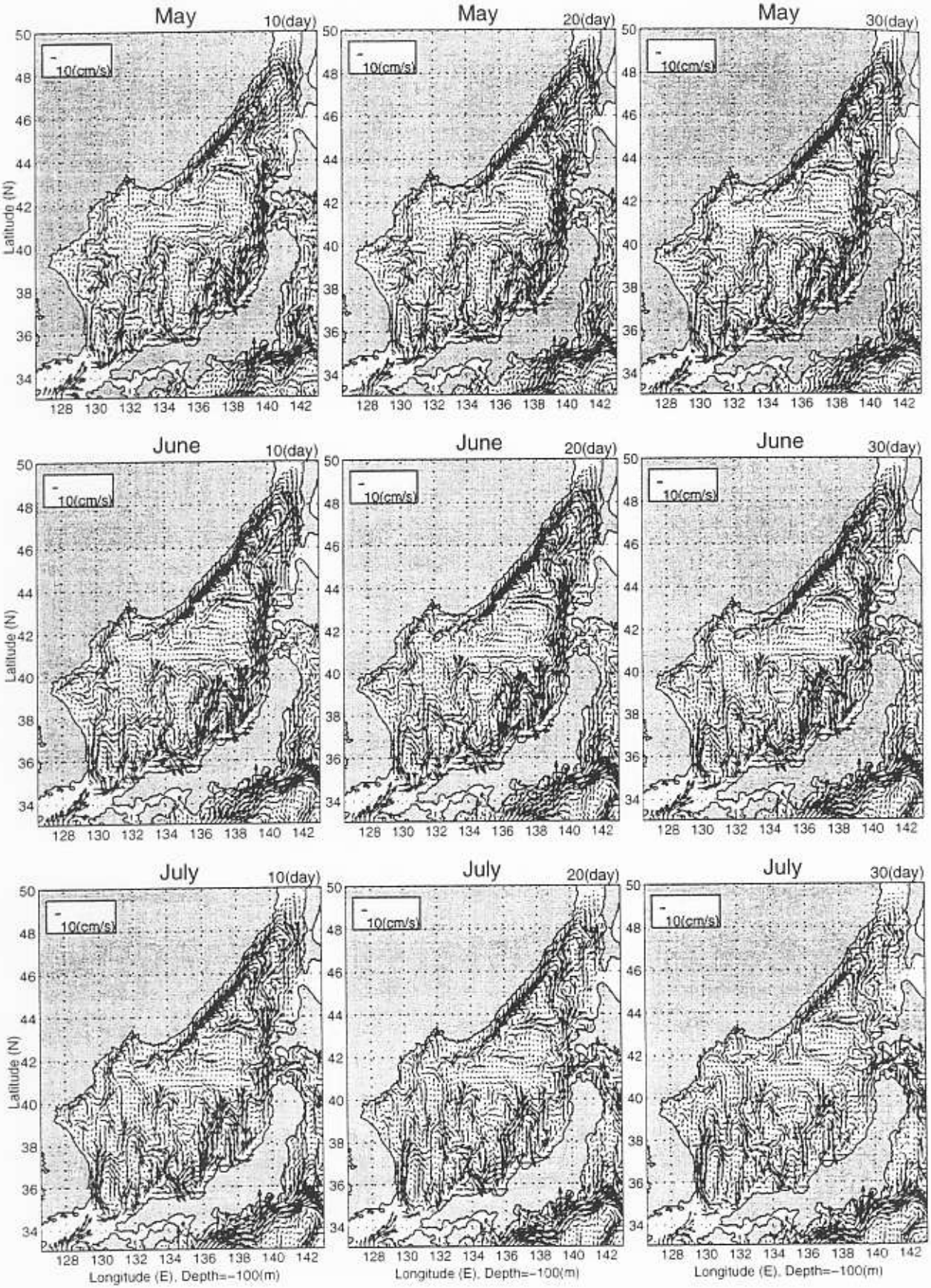


Figure 8 JES circulation at 100 m depth simulated by the nested POM Model.

few days integration. After the 5 days of integration, the peak error velocity show the decaying inertial oscillation superimposed into asymptotic values. The asymptotic value is around 0.19 cm/s for the ordinary scheme and 0.15 cm/s for the compact scheme. For the sixth order difference the asymptotic value is near 0.04 cm/s for the ordinary scheme and 0.02 cm/s for the compact scheme.

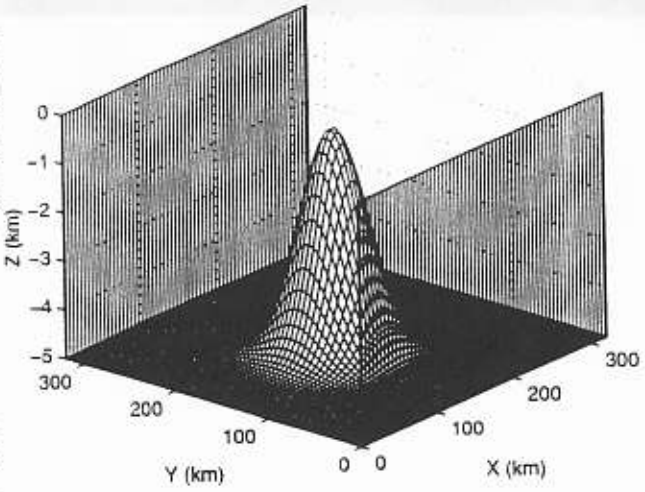


Figure 10 – Seamount geometry (from Chu and Fan, 1997)

## 7 Conclusions

Preparation of accurate boundary conditions is extremely important for ocean prediction. However, the difference among commonly used surface forcing functions (e.g., NSCAT and NCEP surface winds) is not small. Root-mean-square difference over the South China Sea increases from 3.6 m/s 1 November to a maximum value of 6.7 m/s on 4 November 1996, the day when Ernie was formed; and then fluctuates between 6.7 m/s and 2.7 m/s afterwards. The response of the South China Sea to the uncertain surface forcing is also evident. Therefore, it is quite urgent to study the role of boundaries and sensitivity to boundary conditions.

The optimization method provides a useful scheme to obtain unknown open boundary values from known interior values. Different from the adjoint method, this scheme can be easily incorporated into any ocean models. For time-dependent dynamical models, when the temporally varying values are given at interior observation points, the optimization method can be used for each time step to obtain the unknown open boundary values for that time step. For a primitive equation model with turbulent mixing processes (e.g., POM), it is very important to use smoothing on the open boundary parameter vector. The optimization method performs well even when random noises are added to the 'observational' points. This indicates that we can use real-time data to invert for the unknown open boundary values.

The $\sigma$-coordinate, pressure gradient error depends on the choice of difference schemes. By choosing an optimal scheme, the error may be reduced a great deal without increasing the horizontal resolution. Analytical analysis shows that the truncation error of the fourth-order scheme may be 1-2 order of magnitude smaller than the second-order scheme, and the truncation error of the sixth-order scheme may be 1-2 order of magnitude smaller than the fourth-order scheme within the same order of the difference the combined compact scheme leads to a minimum truncation error. The compact scheme may reduce near 55% error, and the combined compact scheme may reduce near 84% error for the sixth order difference.

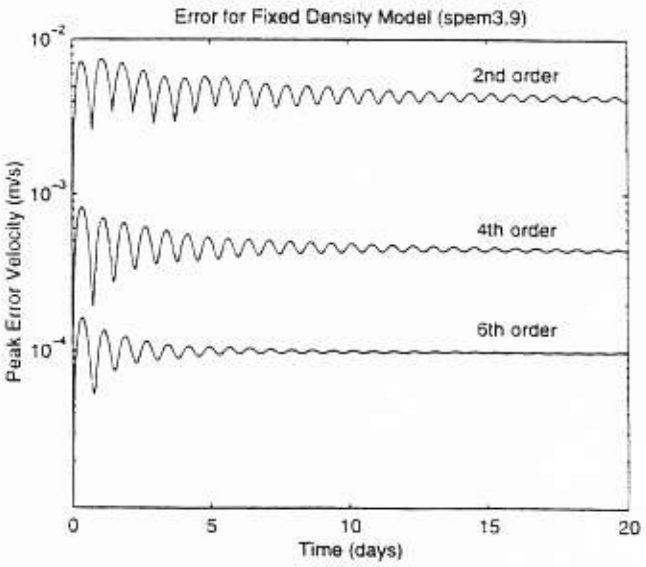


Figure 11 – Peak error velocity for the second, fourth, and sixth order schemes (from Chu and Fan, 1997).

## 8 ACKNOWLEDGMENTS

This research is sponsored by the Office of Naval Research (ONR) Naval Ocean Modeling Program (NOMP). Chenwu Fan, Shihua Lu, Yuchun Chen, and Laura Ehret have contributed significantly to these studies of toward accurate littoral zone modeling.

## REFERENCES

Beckmann, A., and D. B. Haidvogel, 1993: Numerical simulation of flow around a tall isolated seamount. Part 1: Problem formulation and model accuracy. *Journal of Physical Oceanography*, **23**, 1736-1753.

Blumberg, A.F., and G.L. Mellor, 1987: A description of a three-dimensional coastal ocean circulation model. *Three Dimensional Coastal Ocean Models*, edited by N.S. Heaper, American Geophysical Union, 1-16.

Chang, H.R., and H.N. Shirer, 1985: Compact spatial differencing techniques in numerical modeling. *Monthly Weather Review*, **113**, 409-423.

Chapman, D., 1985: Numerical treatment of cross-shelf open boundaries in a barotropic ocean model. *Journal of Physical Oceanography*, **15**, 1060-1075.

Chu, P.C., 1999: Two kinds of predictability in Lorenz system. *Journal of the Atmospheric Sciences*, in press.

Chu, P.C., and C. Fan, 1997: Sixth-order difference scheme for sigma coordinate ocean models. *Journal of Physical Oceanography*, **27**, 2064-2071.

Chu, P.C., C. Fan, and L. Ehret, 1997: Determination of open boundary conditions with an optimization method. *Journal of Atmospheric and Oceanic Technology*, **14**, 723-734.

Chu, P.C., and C. Fan, 1998: A three-point combined compact difference scheme. *Journal of Computational Physics*, **140**, 370-399.

Chu, P.C., Y.C. Chen, and S.H. Lu, 1998a: On Haney-type surface thermal boundary conditions for ocean circulation models. *Journal of Physical Oceanography*, **28**, 890-901.

Chu, P.C., S.H. Lu, W.T. Liu, 1998b: Uncertainty of the South China Sea prediction using NSCAT and NCEP winds during tropical storm Ernie 1996. *Journal of Geophysical Research*, in press.

Chu, P.C., and C. Fan, 1999: A three-point sixth-order nonuniform combined compact difference scheme. *Journal of Computational Physics*, **148**, 663-674.

Gunson, J.R., and P. Malanotte-Rizzoli, 1996: Assimilation studies of open-ocean flows: 1. estimation of initial and boundary conditions. *Journal of Geophysical Research*, **101**, *28,457-28,472*.

Haidvogel, D.B., J.L. Wikin, and R. Young, 1991: A semi-spectral primitive equation model using vertical sigma and orthogonal curvilinear coordinates. *Journal of Computational Physics*, **94**, 151-185.

Haney ,1991: On the pressure gradient force over steep topography in sigma coordinate ocean models. *Journal of Physical Oceanography*, **21**, 610-619.

Hedstrom, K., 1994: User's Manual for a Semi-Spectral Primitive Equation Ocean Circulation Model Version 3.9, Rutgers University, New Jersey.

McCalpin, J.D., 1994: A comparison of second-order and fourth-order pressure gradient algorithms in a $\sigma$-coordinate ocean model. *International Journal for Numerical Methods in Fluids*, **18**, 361-383.

Mellor, G.L., T. Ezer, and L.-Y. Oey, 1994: The pressure gradient conundrum of sigma coordinate ocean models. *Journal of Atmospheric and Oceanic Technology*, **11**, 1126-1134.

Mellor, 1991: User's Guide for A Three Dimensional, Primitive Equation, Numerical Ocean Model. Princeton University.

Oliger, J., and Sundstrom, 1978: Theoretical and practical aspects of some initial boundary value problems in fluid dynamics. *SIAM Journal of Applied Mathematics*, **35** (3), 419-446.

Orlanski, I., 1976: A simple boundary condition for unbounded hyperbolic flows. *Journal of Computational Physics*, **21**, 251-269.

Robinson, A.R., 1993: Physical precesses, field estimation and interdisciplinary ocean modeling. *Harvard Open Ocean Model Reports*, Harvard University, Cambridge, 71 pp.

Seiler, U., 1993: Estimation of the open boundary conditions with the adjoint method. *Journal of Geophysical Research*, **98** (C12), 22855-22870.